

Automatika

Journal for Control, Measurement, Electronics, Computing and Communications



ISSN: (Print) (Online) Journal homepage: www.tandfonline.com/journals/taut20

Local search enhanced optimal Inception-ResNet-v2 for classification of long-term lung diseases in post-COVID-19 patients

Anusha Sanampudi & S. Srinivasan

To cite this article: Anusha Sanampudi & S. Srinivasan (2024) Local search enhanced optimal Inception-ResNet-v2 for classification of long-term lung diseases in post-COVID-19 patients, *Automatika*, 65:2, 473-482, DOI: [10.1080/00051144.2023.2295142](https://doi.org/10.1080/00051144.2023.2295142)

To link to this article: <https://doi.org/10.1080/00051144.2023.2295142>



© 2024 The Author(s). Published by Informa UK Limited, trading as Taylor & Francis Group.



Published online: 15 Jan 2024.



Submit your article to this journal [↗](#)



Article views: 446



View related articles [↗](#)



View Crossmark data [↗](#)



Citing articles: 1 View citing articles [↗](#)



Local search enhanced optimal Inception-ResNet-v2 for classification of long-term lung diseases in post-COVID-19 patients

Anusha Sanampudi^a and S. Srinivasan^b

^aDepartment of Artificial Intelligence and Data Science, R.M.K. Engineering College, Kavaraipettai, India; ^bDepartment of Computer Science and Engineering, R.M.D. Engineering College, Kavaraipettai, India

ABSTRACT

The Coronavirus disease (COVID-19) has emerged as a global epidemic, posing a significant threat to countries worldwide. COVID-19 is closely associated with pneumonia, leading to the unfortunate loss of many lives due to pulmonary conditions. Differentiating between pneumonia and COVID-19 based on chest X-ray images has become a challenging task. This paper proposes a Local Search Enhanced AHO-based Inception-ResNet-v2 Model to develop a robust and accurate classification model for identifying and categorizing chronic lung diseases in patients who have recovered from COVID-19. The proposed model utilizes the Inception-ResNet-v2 architecture to extract features from CT scan images, which are then used to classify the lung diseases present in the patients. A curated dataset of CT scan images from post-COVID-19 patients with known lung disease classes is used to train the model. Experimental results demonstrate that the proposed method achieves an accuracy of 98.97%, precision of 98.95%, sensitivity of 98.91%, F-score of 98.86%, and specificity of 98.89%. These performance metrics are comparable to those achieved by methods based on manually delineated contaminated areas.

ARTICLE HISTORY

Received 28 September 2023
Accepted 8 December 2023

KEYWORDS



COVID-19; lung disease; deep learning; classification; optimization

1. Introduction

Lung diseases are a leading cause of global mortality, encompassing a wide range of conditions such as interstitial lung diseases (ILDs), pulmonary edema, pneumonia, and pulmonary fibrosis, among others [1]. Accurate diagnosis and monitoring of these lung diseases pose significant challenges on a global scale. Computed Tomography (CT) is the conventional imaging technique that plays a crucial role in the diagnosis of lung diseases [2]. The COVID-19 pandemic has raised important research questions regarding the mechanisms involved in pulmonary complications following moderate to severe acute illnesses [3]. There is growing concern about potential long-term pulmonary complications in patients with more severe disease outcomes. In this context, we present the case characterization of four COVID-19 patients who exhibited chronic interstitial lung abnormalities on CT scans taken 90 days after hospital discharge [4]. Patients with severe dyspnea and severe manifestations of the disease often require mechanical ventilation, leading to increased pulmonary sequelae and extensive pulmonary fibrosis. As COVID-19 survivors who develop chronic pulmonary disease require long-term specialized care, mitigating the various risk factors associated with post-COVID-19 complications becomes crucial.

The use of CT scans is crucial in diagnosing lung conditions in patients exhibiting symptoms of COVID-19. CT scanning provides high-resolution images, offering a detailed view of the affected areas and clearer visualization of internal tissues and organs [5]. In individuals with COVID-19, CT scan images often reveal white spots in the lungs, known as ground-glass opacities, which aid radiologists in early detection and diagnosis of the disease [6]. To further enhance the classification of long-term lung diseases in patients who have recovered from COVID-19, we propose the utilization of the Local Search Enhanced AHO-based Inception-ResNet-v2 Model. This model aims to develop a robust and accurate classification system, improving the identification and categorization of various lung conditions in post-COVID-19 patients. The main contribution of the paper is defined as follows:

- Development of an innovative classification model specifically designed for post-COVID-19 patients, effectively addressing the distinctive challenges associated with their long-term lung diseases
- Integration of the Inception-ResNet-v2 architecture as a powerful feature extractor to capture multi-scale features from CT scan images, enabling accurate and comprehensive disease classification.

CONTACT Anusha Sanampudi  anushasanampudi.ai@gmail.com; mailZanushasanampudi@gmail.com  Department of Artificial Intelligence and Data Science, R.M.K. Engineering College, Kavaraipettai, Tamilnadu, India

© 2024 The Author(s). Published by Informa UK Limited, trading as Taylor & Francis Group.

This is an Open Access article distributed under the terms of the Creative Commons Attribution License (<http://creativecommons.org/licenses/by/4.0/>), which permits unrestricted use, distribution, and reproduction in any medium, provided the original work is properly cited. The terms on which this article has been published allow the posting of the Accepted Manuscript in a repository by the author(s) or with their consent.

- Evaluation of the model's performance on a diverse and annotated dataset, showcasing its potential in supporting healthcare professionals in diagnosing and monitoring post-COVID-19 lung diseases.

The rest of the paper is prepared as follows, Section 2 carries the literature review, the proposed technique is defined in Section 3, the results and discussions are offered in Section 4, and the paper is eventually concluded with Section 5.

2. Literature review

Yadav et al. [7] introduced Generative Adversarial Networks (GANs) for categorizing lung diseases. The model utilized multilayer GAN architecture for learning representations of images of different lung diseases. Also stacking classifiers such as linear Support Vector Classification and Random Forest are used for classifying lung diseases through the representations of disease images. As a result, the model provided high sensitivity, identified COVID-19 patients, and distinguished different lung diseases from COVID-19. Meanwhile, for enhancing the classification performance of the model, a new loss function was required to combine the stacking classifier and GAN.

Hasan et al. [8] proposed a feature extraction model, known as QDE-DF (Q-Deformed Entropy and Deep Learning Features), to improve the classification process of pneumonia, CT lung scans, and COVID-19. This model includes pre-processing steps to mitigate the impact of CT slice variations. The extracted features are then classified using long short-term memory (LSTM). Experimental analysis demonstrates that the proposed model outperforms existing methods, although it is noted to be computationally expensive.

In a study by Zhang et al. [9], a relation-driven collaborative learning model was developed to enhance the overall performance of COVID-19 infection classification, especially in scenarios with limited training data. The results show that their approach achieves superior segmentation performance compared to other methods, even in the absence of sufficient COVID-19 data. However, it is important to note that the effectiveness of transfer learning can be compromised when datasets exhibit substantial differences in domain or characteristics.

Xiao et al. [10] introduced a slice forecasting model called PAM-DenseNet, which incorporates a dense connectivity network with a parallel attention module. The pre-trained model is then applied to a dataset of CT scans to obtain patient-wise predictions using a vote-casting mechanism. Experimental results demonstrate that the proposed approach achieves promising outcomes in terms of accuracy, precision, sensitivity, and specificity, comparable to methods based on manual delineation of affected areas. Manual delineation is a

time-consuming and labor-intensive process, which is further exacerbated by the excessive workload faced by clinicians during the pandemic.

An et al. [11] proposed a multi-scale adversarial domain adaptation network (MS-AdaNet) to enhance the task of cross-sectional lung segmentation, leveraging previous knowledge from the categorization network. The challenges posed by domain shift problems, variations in imaging configurations, modalities, and other factors hinder the overall performance and progress of lung segmentation.

In another study, Fan et al. [12] introduced the COVID-19 Lung Infection Segmentation Deep Network (Inf-Net) for automatic detection of infected areas in chest CT slices. Additionally, they constructed a semi-supervised COVID-SemiSeg dataset. Extensive experiments conducted on both the COVID-SemiSeg dataset and real CT volumes demonstrate that Inf-Net outperforms most state-of-the-art segmentation models and improves upon existing performance. The detection of variations in infection size and characteristics in CT slices poses a significant challenge.

2.1. Research gaps

Limited Focus on Post-COVID-19 Lung Diseases: While there is growing research on the acute phase of COVID-19 and its impact on the lungs, there is a relative scarcity of studies specifically addressing long-term lung diseases that persist in post-COVID-19 patients. Investigating and classifying these long-term lung diseases can provide valuable insights into patient care and treatment strategies.

Lack of Comprehensive Classification Models: Existing studies on lung disease classification often focus on specific diseases or limited categories. There is a need for more comprehensive classification models that encompass a wide range of long-term lung diseases observed in post-COVID-19 patients. Developing a robust and accurate classification model that covers diverse lung conditions can aid in early detection, monitoring, and personalized treatment.

Interpretability and Explainability of Classification Models: Many Models often exhibit high performance but lack interpretability. Developing methods to explain the model's predictions and highlight relevant image features can improve the acceptance and adoption of classification models in clinical settings.

3. Proposed local search enhanced AHO-based Inception-ResNet-v2 model

This section offers step-by-step records of the proposed technique for robust and effective categorization of Covid-19 sickness from input chest CT scan images. Figure 1 represents the proposed IRV2-LSEAH architecture. This includes the raw chest CT scan images,

the ROI of the lung region, particular feature extraction, feature fusion, and normalization methods for discovery and categorization. The result provides the detection and classification of lung disease. The normalized and fused features of the sample forecast the lung diseases into viral pneumonia, bacterial pneumonia, and normal varieties. The proposed system aims to develop a robust and accurate classification model for identifying and classifying long-term lung diseases in patients who have recovered from COVID-19. This system utilizes the Inception-ResNet-v2 model for extraction of feature from CT scan images. The features extracted are then used to classify the lung diseases present in the patients. The system begins with the pre-processing of CT scan images, which involves resizing, normalization, and potentially applying adaptive filtering techniques to enhance the quality of the lung structures. The pre-processed images are then fed into the Inception-ResNet-v2 model for extraction of features. The Inception-ResNet-v2 model, with its combination of convolutional layers, Inception modules, and residual connections, is capable of capturing intricate patterns and relevant features from the CT scan images. By removing the fully connected layers and employing global average pooling, the model extracts high-level features that represent the unique characteristics of the lung diseases. A classification layer, consisting of fully connected layers followed by a softmax activation function, is added on top of the global average pooling layer. This layer maps the extracted features to the specific lung disease classes and assigns probability scores to each class. To train the model, a labelled dataset of CT scan images from post-COVID-19 patients with known lung disease classes is utilized. After training, the model undergoes evaluation on a separate validation dataset to assess its performance and generalization ability. Fine-tuning is applied to optimize the model's hyperparameters, ensuring optimal accuracy and robustness. Once the model achieves satisfactory performance, it is tested to evaluate its effectiveness in classifying long-term lung diseases in post-COVID-19 patients. The ultimate goal is to deploy the model in clinical settings, where it can assist healthcare professionals in diagnosing and monitoring lung diseases, leading to improved patient care and outcomes.

3.1. Pre-processing stage

Pre-processing the CT scan images is an essential step before using them for classification with the Inception-ResNet-v2 model. This step involves several operations to prepare the images for analysis.

Image Resizing: CT scan images can have varying resolutions, and it is important to ensure consistency in the image sizes. Resizing involves adjusting the dimensions of the images to a predetermined size. This step ensures that all images have the same width and height, which is

important for feeding them into the Inception-ResNet-v2 model.

Intensity Normalization: CT scan images often have varying pixel intensities due to differences in acquisition protocols or equipment. Intensity normalization is performed to standardize the pixel values across the images. This step brings the pixel intensities to a common range, such as scaling them between 0 and 1, to ensure that the model can effectively learn from the data.

Image Enhancement: Adaptive filtering techniques aim to enhance image quality by reducing noise while preserving important structures.

3.2. Adaptive median filtering

The median filter eliminates the noise in the image and from this, it maintains the image's sharpness [13]. The median value of nearer pixels changes every pixel and 3×3 window is employed. This filter eliminates the speckle noise and is the finest filter in conventional filters. The adaptive median filter retains the edges and structure of the image. According to every pixel, the window size differs in the adaptive median filter. if the adaptive median filter increased, structural metrics would be slightly reduced, by this an image will be somewhat blurred. The below equation represents the probability density function:

$$P(y) \begin{cases} pu, y = u \\ pv, y = v \\ 0, \text{ other} \end{cases} \quad (1)$$

From the above equation, pu and pv are specified as probability related to u and v , and the $u = 0$ and $v = 255$ are the black-and-white noise points. The following equation indicates the median filter expression:

$$L(j, i) = \text{Median}(m(s)) \quad (2)$$

where, m represented as the sort of gray value sequences, s specified as the number of pixels, i denoted as the pixel vertical coordinate, and j represented as the pixel horizontal coordinates. If the noise probability $p(y) > 20$, the filtering effect would decrease in the traditional median filter. The noise point replaces the median point if the window incorrect noise point is higher than 50%, this generates the importance of filter loss. The adaptive median filter determines the condition for differentiating whether the replaced median filter is a noise point or not and this will be beneficial for avoiding the issue of median filter.

3.3. Feature extraction with Inception-ResNet-v2

Feature extraction with the Inception-ResNet-v2 model involves utilizing its convolutional layers for extracting high-level features from the preprocessed CT scan images.

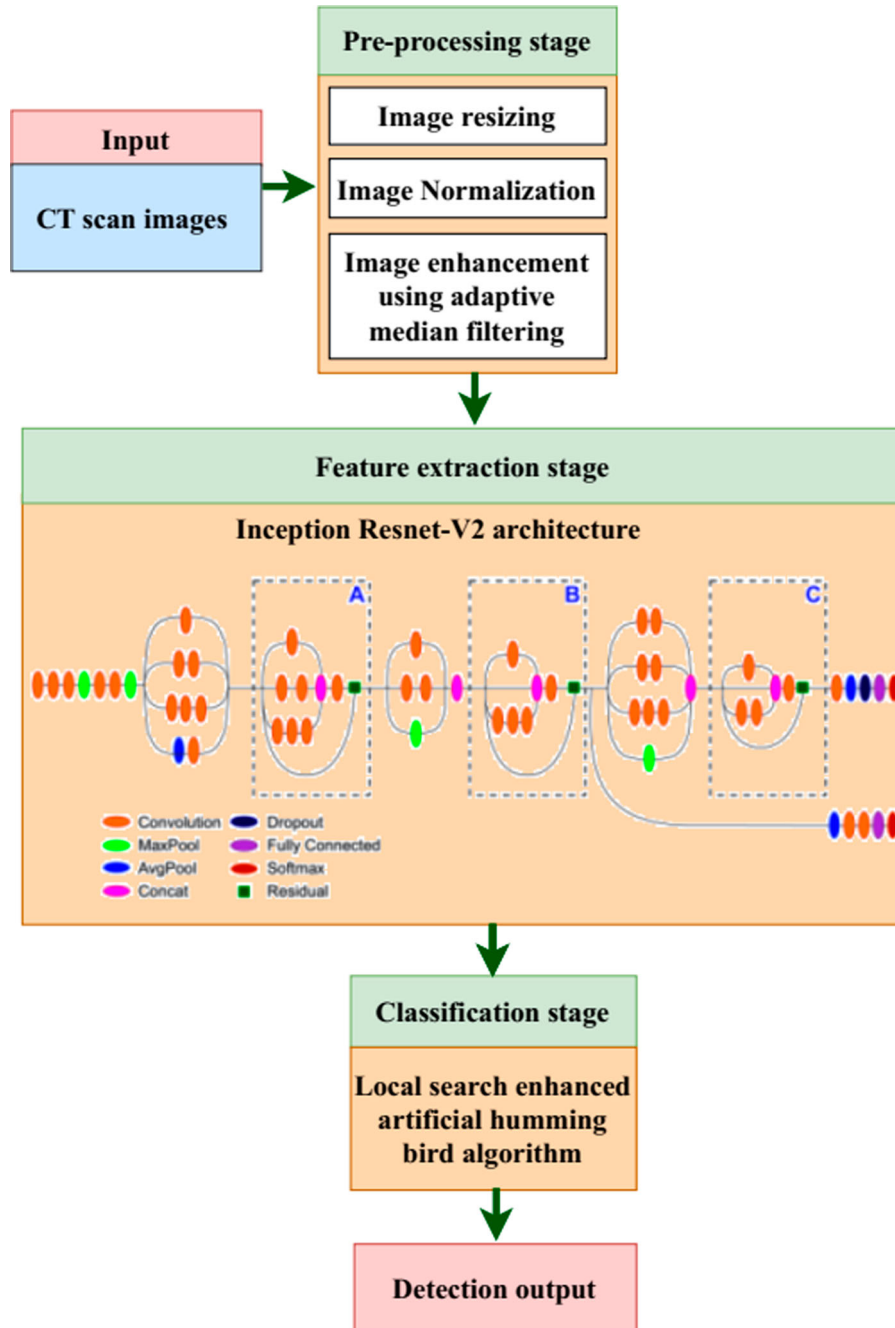


Figure 1. Overall architecture.

Convolutional Layers: The Inception-ResNet-v2 model consists of multiple convolutional layers arranged in a deep network architecture. These layers are designed to learn and capture meaningful visual features at different scales and levels of abstraction. Each convolutional layer applies a set of filters or kernels to the input image, performing local feature detection. From the prior layer mapping and determining the local connections of features is the primary objective of the convolutional layer. The below equation shows the convolutional operation of the input, which is denoted as J for the filter $F \in \mathbb{R}^{2x_1+2y_2}$.

$$(J * F)_{m,n} = \sum_{g=-x_1}^{x_1} \sum_{i=-x_2}^{y_2} F_{g,i} J_{m-g,n-i} \quad (3)$$

$$\text{filter } F \text{ is } \begin{bmatrix} F_{-x_1,-x_2} & \cdots & F_{-x_1,x_2} \\ \vdots & F_{0,0} & \vdots \\ F_{x_1,-x_2} & \cdots & F_{x_1,x_2} \end{bmatrix} \quad (4)$$

Relu is the activation function, which is employed in the feature map.

Hierarchical Feature Representation: As the pre-processed CT scan images are fed through the Inception-ResNet-v2 model, they pass through the convolutional layers sequentially. Each layer extracts increasingly complex and abstract features from the input images. Lower layers capture low-level features like edges, corners, and textures, while higher layers capture more sophisticated structures and patterns specific to lung diseases.

Inception-ResNet-v2 Architecture: The Inception-ResNet-v2 model incorporates inception modules, which are key components that allow for multi-scale feature extraction. These modules consist of parallel convolutional branches with different filter sizes, enabling the model to capture features at various receptive fields. The residual connections in the Inception-ResNet-v2 architecture help mitigate the vanishing gradient problem, allowing for effective training of deep networks. The Inception network structure assumes that taking out a number of features from the various scales and different convolution kernels of sizes in various are able to enhance network adaptability [13]. This network is able to decrease certain convolution kernels, which can diminish the model's complexity. Transmitting the signals of several units for each layer backward or forward, this process expedites parameter optimization and training of the network. There is a need to utilize 1×1 convolution for decreasing or enhancing the dimension because the feature map y_h might be a variant in the residual convolution network. The below equation specifies the residual operation:

$$F(y_h) = e * y_h + \beta \quad (5)$$

$$x_h = Rl(F) + s(y_h) \quad (6)$$

$$y_{h+1} = Rl(x_h) \quad (7)$$

where β represented as the offset, y_h denoted as the input, the sum of the two branches is represented as the x_h , e denoted as the weight, Rl denoted as the *relu* function, the convolutional operation is indicated as $F(y_h)$, y_{h+1} denoted as the final output of the residual module, and $s(y_h)$ is specified as the simple transformation for the input.

$$Rl(y) = \max i(0, y) \quad (8)$$

use y value and threshold of 0 as input in the calculation of forward and can acquire the output. Avoiding the issue regarding the gradient disappearing in the process of the Inception network model training phase, and this is the primary aim of the residual network learning unit. If the network model has achieved a specific saturation, this layer could be mapped similarly, and this will help to train the network rapidly and simply.

$$\frac{\alpha Y_m}{\alpha Y_j} = \frac{\alpha Y_j + F(Y_j, \tau_j, \beta_j)}{\alpha Y_j} = 1 + \frac{\alpha F(Y_m, \tau_m, \beta_m)}{\alpha Y_m} \quad (9)$$

The above equation Y_j indicates the input of the j th residual unit, the input of the m th unit is denoted as the Y_m residual function specified as the $F(\cdot)$.

Feature Map Extraction: At each convolutional layer, the model generates a set of feature maps or activation maps. Every feature map signifies the response of a particular filter to the input image. These maps highlight areas in the image where certain features or patterns

are present. The deeper the layer, the higher the level of abstraction captured in the feature maps.

Dimensionality Reduction: To reduce the computational complexity and facilitate efficient feature representation, the Inception-ResNet-v2 model incorporates dimensionality reduction technique. This is typically achieved through techniques such as 1×1 pooling operations. Dimensionality reduction minimizes the spatial dimensions of the feature maps while preserving the important features.

3.4. Global average pooling

After the feature extraction layers, a global average pooling operation is applied. This operation minimizes the spatial dimensions of the feature maps to a fixed size, generating a fixed-length feature vector for each CT scan image. Global average pooling calculates the average value within each feature map, preserving important information about the distribution of features while reducing spatial redundancy. The GAP filter computes the value of the global average from every output feature map [14]. 1×1 is the size of the output feature map.

$$G_{avg-pooling}^j = \frac{1}{3} \sum_{j=1}^e Y_{1:g,1:p,j}^j \quad (10)$$

In this, j represented as the index of the output feature maps, $G_{avg-pooling}$ denoted as the output feature map's global average pooling, e denoted as the total number of element values, $Y_{1:g,1:p,j}$ specifies the element value associated with the global average pooling filter.

3.5. Classification layer

After the global average pooling layer, a classification layer is added to perform the final classification. This layer is responsible for mapping the extracted features to the specific lung disease classes present in the dataset. It consists of fully connected layers, which are densely connected neural network layers. The fully connected layers learn to capture the relationships and patterns in the extracted features and map them to the appropriate lung disease classes. Each neuron in the fully connected layers represents a learned weight associated with a specific feature. The output of these neurons is determined by applying a nonlinear activation function, such as the rectified linear unit (ReLU), to the weighted sum of inputs. The final layer of the classification layer is typically a softmax activation function. The softmax function assigns probability scores to each lung disease class based on the learned features. These probability scores indicate the model's confidence in the presence of each disease class for a given input CT scan image. The class with the highest probability score is considered as the predicted class label. The below equation

represents the Fully connected operators:

$$f(y) := E_k y + a_k \quad (11)$$

In this, a_k denoted as the bias vector, E_k represented as the weight in the layer k , y represented as the input layer from the prior layer. In every input, the activation operator uses an activation function.

3.6. Artificial hummingbird algorithm (AHA)

This section describes the artificial hummingbird algorithm (AHA), which is based on the clever characteristics of hummingbirds [15]. The hummingbird analyzes multiple numbers of food sources to choose a suitable food source. Every hummingbird always remembers the particular source of food allocated to it. The food collection data of multiple hummingbirds are saved in the visit table.

3.6.1. Initialization

The process is initiated by placing m humming birds on m sources of food.

$$c_r = Low + i.(Up - Low)r = 1, \dots, \quad (12)$$

Here, the d-dimensional issue's upper and lower limits are mentioned by Up and Low . A random vector in the range $[0, 1]$ is indicated by i , and the provided issue's solution r th food source's location is denoted by c_r .

- Guided foraging

Hummingbirds naturally possess the talent of finding the source of food which contains a maximum amount of nectar. In the AHA algorithm axial, omnidirectional, and diagonal are the three flight skills utilized at the time of foraging and using a direction switch vector they are designed.

The axial flight in the $w - W$ space is given below:

$$W^{(r)} = \begin{cases} 1 & \text{if } r = randi([1, w]) \\ 0 & \text{else} \end{cases} \quad r = 1, \dots, w \quad (13)$$

The diagonal flight is described below:

$$W^{(r)} = \begin{cases} 1 & \text{if } r = k(q), q \in [1, p], \\ & k = randperm(p), \\ & p \in [2, \lceil i_1 \cdot (w - 2) \rceil + 1] \\ 0 & \text{else} \end{cases} \quad i = 1, \dots, w \quad (14)$$

The description of the omnidirectional flight is given below:

$$W^{(r)} = 1 \quad r = 1, \dots, w \quad (15)$$

Here, from 1 to w a random number is created by $randi([1, w])$, from 1 to p an uneven permutation of

integers is generated by $randperm(p)$, and a random number in the interval $(0, 1]$ is i_1 . The derivation of a candidate food source and the mathematical equation used in the simulation of the characteristics of foraging which is guided is given below:

$$E_r = (g + 1) = c_{r,tar}(g) + z.W.(c_r(g) - c_{r,tar}(g)) \quad (16)$$

$$z \sim M(0,1) \quad (17)$$

Here, at time g the location of the r th food source is $c_r(g)$, the location of the food source the r th hummingbird thinks to visit is $c_{r,tar}(g)$, and the guided factor that undergoes normal distribution $M(0, 1)$ is a . The r th food source's location update is given below:

$$c_r(g + 1) = \begin{cases} c_r(g) & u(c_r(g)) \leq u(e_r(g + 1)) \\ e_r(g + 1) & u(c_r(g)) > u(e_r(g + 1)) \end{cases} \quad (18)$$

Here, the value of function fitness is indicated by $u(\cdot)$.

- Territorial foraging

When, the targeted food source is eaten completely, the hummingbird searches for a new source of food inside its region. The hummingbird's local search is mathematically expressed as:

$$e_r(g + 1) = c_r(g) + y.W.c_r(g) \quad (19)$$

$$y \sim M(0,1) \quad (20)$$

Here, the territorial factor that undergoes normal distribution $M(0, 1)$ is y . The migration from a hummingbird to a randomly produced new one with the worst nectar-refilling charge may be given as:

$$C_{worst}(g + 1) = LOW + i.(UP - LOW) \quad (21)$$

where C_{worst} is the food supply with the worst nectar replenishment rate in the populace. Assuming a 50% opportunity between both guided foraging and regional foraging, guided foraging has an equal likelihood of visiting each of the different sources. Thus, a hummingbird after performing $2m$ repetitions in the worst case, may move to an equivalent food supply as its target source. At this stage, the migration approach should be completed to increase the stagnation and discover the hunting ground.

$$N = 2m \quad (22)$$

The computational complexity is associated with initialization, the health evaluation (x_{eval}), the hummingbird population size (N_{size}), the most range of iterations

(T_{\max}), and the measurement of variables (d_{var}). Then,

$$\begin{aligned} O(\text{AHO}) &= O(\text{problemdefinition}) + O(\text{initialization}) \\ &+ O(g(\text{evaluationfunction})) \\ &+ O(g(\text{guidedforaging})) + O(g(\text{teritorialforaging})) \\ &+ O(g(\text{migrationforaging})) \\ &= O(1 + mw + Gxm + \frac{1}{2}Gmw + \frac{1}{2}Gmw\frac{G}{2m}mx) \\ &\cong O(Gxm + Gmw + \frac{Gw}{2}) \end{aligned} \quad (23)$$

- Searching characteristics

Two test functions are used to prove the searching characteristics of AHA. Rosenbrock, a unimodal function is the first function. $c = (1, 1)$ with $u(c) = 0$ is the optimal solution for this function. Rastrigin function is the second function and $c = (0, 0)$ with $u(c) = 0$ is its optimal solution.

3.7. Hyperparameter tuning using local search enhanced artificial hummingbird optimization (LSAH)

The evaluation and fine-tuning steps are iterative processes that help refine the model and ensure its robustness in classifying long-term lung diseases in post-COVID-19 patients. By incorporating local search steps in AHO can provide a more refined exploration of the hyperparameter space. Hence we applied Local Search Enhanced Artificial Hummingbird Optimization to tune the hyperparameters of the Inception-ResNet-v2 model for classifying long-term lung diseases from COVID-19 CT scan images. By utilizing the power of AHO and local search, we can efficiently navigate the hyperparameter landscape and achieve improved performance for accurate diagnosis and prognosis of lung diseases associated with COVID-19. The mathematical expression in determining the local search capability is obtained as follows.

$$N_S = C + \alpha * \Delta s \quad (24)$$

From the above equation, the updated solution after local search is denoted by, N_S signifies the current solution selected from the population. α denotes the parameter that controls the step size or magnitude of the local search. Δs denotes the change in solution.

4. Results and discussions

This section discusses the results obtained from the study highlighting the effectiveness of the proposed IRV2-LSEAH method. The proposed IRV2-LSEAH method is assessed with various metrics and these results are compared with existing methods such as

Table 1. Parameter settings.

Parameters	Values
Data Samples	2900
Normal	1340
Viral pneumonia	740
Bacterial pneumonia	600
COVID-19	220
Samples for training	80%
Samples for testing	20%

GAN [7], QDE-DF [8], PAM-DenseNet [10], MS-AdaNet [11] and Inf-Net [12].

4.1. Experimental setup

In this study, we simulated the proposed IRV2-LSEAH model using MATLAB with the aim of aiding health-care professionals in the diagnosis and monitoring of lung diseases. The model utilizes the Inception-ResNet-v2 architecture for feature extraction, where the convolutional layers are employed to extract high-level features from CT scan images that have been preprocessed. Following the feature extraction process, a global average pooling operation is applied to retain essential information regarding the distribution of features while reducing spatial redundancy. Finally, a classification layer is added to perform the ultimate classification task.

4.2. Parameter settings

In this study, a dataset of CT scan images from post-COVID-19 patients was collected for analysis. The dataset consisted of a total of 2900 data samples, which were categorized into four classes: normal, viral pneumonia affected, bacterial pneumonia affected, and COVID-19 affected. To evaluate the proposed IRV2-LSEAH method, the dataset was split into training and testing sets, with a ratio of 80:20, respectively. Table 1 provides the parameter settings used in the proposed IRV2-LSEAH method.

4.3. Evaluation measures

For evaluating the proposed model in the classification of long-term lung diseases, various performance metrics are used. The presence and absence of long-term lung disease in a patient are measured using *TruePositive* and *TrueNegative*. The number of wrong detection by the proposed IRV2-LSEAH model is measured using *FalsePositive* and *FalseNegative*.

Accuracy: The mathematical representation of the accuracy is given below:

$$\text{Accuracy} = \frac{(\text{TruePositive} + \text{TrueNegative})}{(\text{TruePositive} + \text{FalsePositive} + \text{TrueNegative} + \text{FalseNegative})} \quad (25)$$

Precision: The equation for the calculation of precision is given below:

$$\text{Precision} = \frac{\text{TruePositive}}{(\text{TruePositive} + \text{FalsePositive})} \quad (26)$$

Sensitivity: Recall is the ratio of true positive to the summation of false negative and true positive. The following equation is used to measure the recall:

$$\text{Recall} = \frac{\text{TruePositive}}{(\text{TruePositive} + \text{FalseNegative})} \quad (27)$$

Specificity: It is the ratio of true negative to the sum of true negative and false positive. It is mathematically expressed as:

$$\text{Specificity} = \frac{\text{TrueNegative}}{(\text{TrueNegative} + \text{FalsePositive})} \quad (28)$$

F-measure: F-measure is referred as the harmonic mean of recall and precision. F-measure combines recall and precision. The below given equation is used to measure the F1-score.

$$\text{F1-score} = 2 \times \frac{(\text{Precision} \times \text{Recall})}{(\text{Precision} + \text{Recall})} \quad (29)$$

4.4. Dataset description

In this work, the data is collected from a labeled dataset of CT scan images from post-COVID-19 patients with known lung disease classes. The dataset consists of 2900 samples in four different categories namely normal class, viral pneumonia affected class, bacterial pneumonia affected class and Covid-19 affected class. Before using the CT scan images for classification with the Inception-RESNET-V2 model, pre-processing them is a crucial step. This step involves operations such as resizing images, intensity normalization, and image enhancement for preparing the images for analysis. CT scan images can have varying resolutions and it is essential to ensure consistency in the image sizes. Resizing involves adjusting the dimensions of the images to a predetermined size. CT scan images have varying pixel intensities due to differences in acquisition protocols. Intensity normalization is implemented to standardize the pixel values across the images. Adaptive filtering techniques are used to improve image quality by reducing noise.

4.5. Performance analysis

Performance analysis is conducted for predicting the best performances of the proposed IRV2-LSEAH method. The performance is evaluated by comparing the proposed IRV2-LSEAH method with the existing methods such as GAN, QDE-DF, PAM-DenseNet, MS-AdaNet, and Inf-Net. Figure 2 shows the accuracy

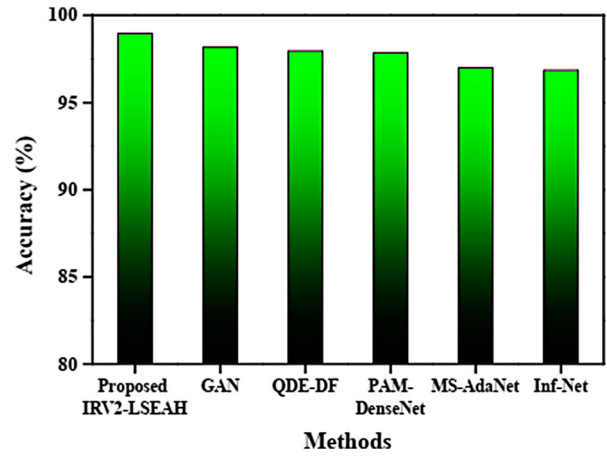


Figure 2. Accuracy analysis.

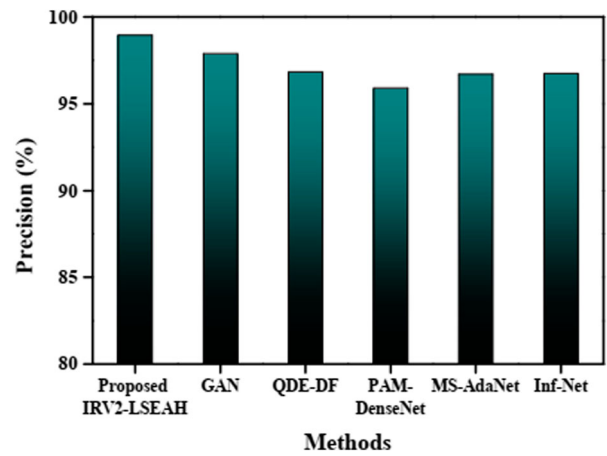


Figure 3. Precision analysis.

analysis of existing methods and the proposed IRV2-LSEAH method. The proposed IRV2-LSEAH method and Inf-Net achieved a higher and lower accuracy of 98.97% and 96.84%, respectively. From this accuracy analysis, the proposed IRV2-LSEAH method attained a better performance compared to other methods. The accuracy of 98.16%, 97.95%, 97.86%, and 96.99% is obtained from GAN, QDE-DF, PAM-DenseNet, and MS-AdaNet, respectively.

Figure 3 represents the precision analysis of existing methods and the proposed IRV2-LSEAH method. Among all these methods the proposed IRV2-LSEAH method achieved a high precision of 98.95% which denotes the best performance. The existing methods such as GAN, QDE-DF, PAM-DenseNet, MS-AdaNet, and Inf-Net obtain a precision of 97.89%, 96.85%, 95.92%, 96.71%, and 96.76%, respectively. From this precision analysis, the proposed IRV2-LSEAH method attained a better performance compared to other methods.

Figure 4 portrays the sensitivity analysis of existing methods and the proposed IRV2-LSEAH method. The proposed IRV2-LSEAH method and PAM-DenseNet method achieved a higher and lower sensitivity of

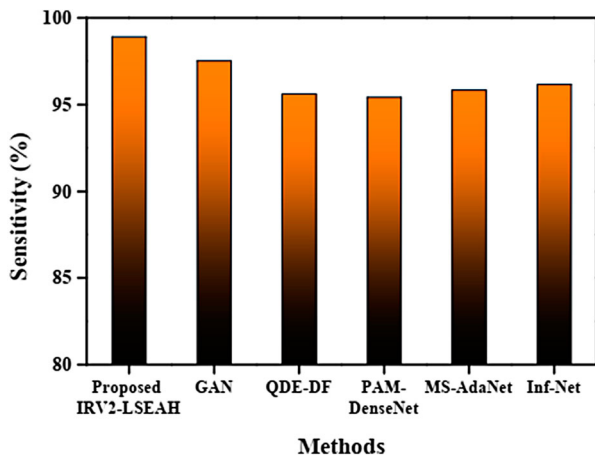


Figure 4. Sensitivity analysis.

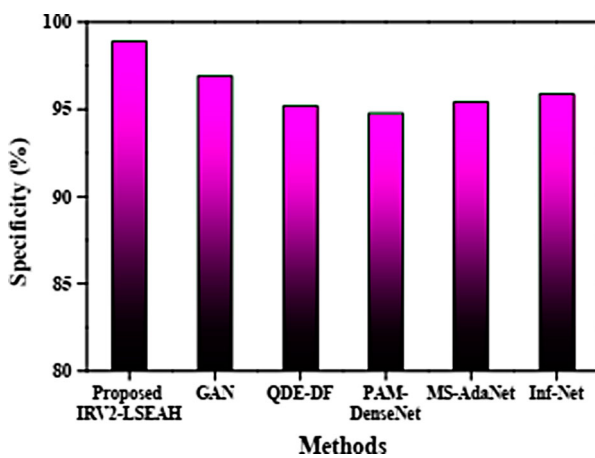


Figure 5. Specificity analysis.

98.91% and 95.43%, respectively. The sensitivity of 97.52%, 95.62%, 95.84%, and 96.17% is obtained from the GAN, QDE-DF, MS-AdaNet, and Inf-Net, respectively. Figure 5 demonstrates the specificity analysis of existing methods and the proposed IRV2-LSEAH method. The proposed IRV2-LSEAH method and PAM-DenseNet method achieved a higher and lower specificity of 98.89% and 94.78%, respectively. The specificity of 96.91%, 95.20%, 95.43%, and 95.87% is obtained from the GAN, QDE-DF, MS-AdaNet, and Inf-Net, respectively. Figure 6 represents the F1-score analysis of existing methods and the proposed IRV2-LSEAH method. The proposed IRV2-LSEAH method and PAM-DenseNet method achieved a higher and lower F1-score of 98.86% and 94.67%, respectively. The F1-score of 94.72%, 94.74%, 95.27%, and 95.54% is obtained from the GAN, QDE-DF, MS-AdaNet, and Inf-Net, respectively.

5. Conclusion

The COVID-19 pandemic has had a global impact and accurate assessment of the disease is crucial. Computed Tomography (CT) plays a significant role in quantitatively assessing COVID-19, particularly in

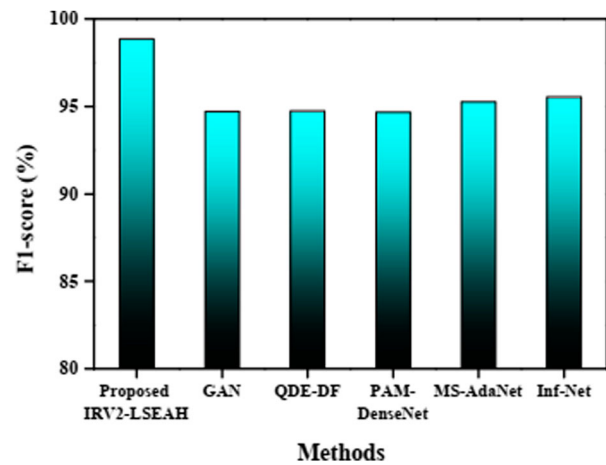


Figure 6. F1-score analysis.

automated lung contamination segmentation. However, segmenting inflamed areas from CT images faces several challenges, including variations in contaminant properties and limited differentiation between infected and normal tissue. To address these challenges, this research proposes a novel method called Inception-ResNet-v2-Local Search Enhanced Artificial Hummingbird (IRV2-LSEAH). The proposed method utilizes a dataset of CT scan images from post-COVID-19 patients and employs various performance evaluation measures. The performance of the proposed IRV2-LSEAH method is evaluated by comparing it with existing methods such as GAN, QDE-DF, PAM-DenseNet, MS-AdaNet, and Inf-Net. The results show that the IRV2-LSEAH method achieves an accuracy of 98.97%, precision of 98.95%, sensitivity of 98.91%, specificity of 98.89%, and F1-score of 98.86%. These performance metrics indicate that the proposed method outperforms the existing methods. In the future, the proposed IRV2-LSEAH model can be further enhanced to detect the severity of the disease, providing valuable insights for healthcare professionals in managing and treating COVID-19 patients.

Disclosure statement

No potential conflict of interest was reported by the author(s).

References

- [1] El-Kenawy ESM, Ibrahim A, Mirjalili S, et al. Novel feature selection and voting classifier algorithms for COVID-19 classification in CT images. *IEEE Access*. 2020;8:179317–179335.
- [2] Zhou B, Yang X, Zhang X, et al. Ultrasound elastography for lung disease assessment. *IEEE Trans Ultrason Ferroelectr Freq Control*. 2020;67(11):2249–2257.
- [3] Xie W, Jacobs C, Charbonnier JP, et al. Relational modeling for robust and efficient pulmonary lobe segmentation in CT scans. *IEEE Trans Med Imaging*. 2020;39(8):2664–2675.

- [4] Ambardar SR, Hightower SL, Huprikar NA, et al. Post-COVID-19 pulmonary fibrosis: novel sequelae of the current pandemic. *J Clin Med.* 2021;10(11):2452.
- [5] Rohmah, L.N. and Bustamam, A., 2020, November. Improved classification of coronavirus disease (COVID-19) based on combination of texture features using CT scan and X-ray images. In 2020 3rd international conference on information and communications technology (ICOIACT) (pp. 105–109). Yogyakarta, Indonesia. doi:10.1109/ICOIACT50329.2020.9332123.
- [6] Zhang Q, Zhou J, Zhang B, et al. Automatic epicardial fat segmentation and quantification of CT scans using dual U-nets with a morphological processing layer. *IEEE Access.* 2020;8:128032–128041.
- [7] Yadav P, Menon N, Ravi V, et al. Lung-GANs: unsupervised representation learning for lung disease classification using chest CT and X-ray images. *IEEE Trans Eng Manage.* 2021;70(8):2774–2786.
- [8] Hasan AM, Al-Jawad MM, Jalab HA, et al. Classification of COVID-19 coronavirus, pneumonia and healthy lungs in CT scans using Q-deformed entropy and deep learning features. *Entropy.* 2020;22(5):1–15.
- [9] Zhang Y, Liao Q, Yuan L, et al. Exploiting shared knowledge from non-COVID lesions for annotation-efficient COVID-19 CT lung infection segmentation. *IEEE J Biomed Health Inform.* 2021;25(11):4152–4162.
- [10] Xiao B, Yang Z, Qiu X, et al. PAM-DenseNet: A deep convolutional neural network for computer-aided COVID-19 diagnosis. *IEEE Trans Cybernet.* 2021;52(11):12163–12174.
- [11] An J, Cai Q, Qu Z, et al. COVID-19 screening in chest X-ray images using lung region priors. *IEEE J Biomed Health Inform.* 2021;25(11):4119–4127.
- [12] Fan DP, Zhou T, Ji GP, et al. Inf-net: automatic COVID-19 lung infection segmentation from CT images. *IEEE Trans Med Imaging.* 2020;39(8):2626–2637.
- [13] Wang J, He X, Faming S, et al. A real-time bridge crack detection method based on an improved Inception-ResNet-v2 structure. *IEEE Access.* 2021;9:93209–93223.
- [14] Gong W, Chen H, Zhang Z, et al. A data-driven-based fault diagnosis approach for electrical power DC-DC inverter by using modified convolutional neural network with global average pooling and 2-D feature image. *IEEE Access.* 2020;8:73677–73697.
- [15] Zhao W, Wang L, Mirjalili S. Artificial hummingbird algorithm: a new bio-inspired optimizer with its engineering applications. *Comput Methods Appl Mech Eng.* 2022;388:114194. doi:10.1016/j.cma.2021.114194.